Three-dimensional mathematical modelling of magnetic bead interactions within a magnetic separation system

Olayinka Oduwole, Steve Sheard.

Department of Engineering Science, University of Oxford, Parks Road, Oxford, OX1 3PJ, United Kingdom.

Abstract

Magnetic separation relates to the ability to separate particles based on their magnetic mobilities. This is often limited by the formation of bead agglomerates. Bead agglomerates are formed as a result of attractive magnetic induced interactions among magnetic beads suspended in fluid. A three-dimensional model of the interactions among three equal sized super-paramagnetic beads suspended in a static fluid within a uniform magnetic field is presented here. The beads' trajectories were recorded on video while the relative axial displacement of the bead was obtained using the recorded off-focus images. A good agreement was obtained by comparing the beads' simulated trajectories with the video data. Therefore, the model is able to predict the behaviour of magnetic beads in immunoassays as well as magnetic separation system.

Keywords: Super-paramagnetic bead; Magnetic Interaction; Hydrodynamic Interaction; Immunoassay; Magnetic separation; Three-dimensional model.

1. Introduction

Super-paramagnetic beads are made of a core which consists of nano-particles (magnetic iron oxide) embedded within a spherical matrix [1, 2]. The large surface to volume ratio of super-paramagnetic beads (or particles) allow for easy attachment to specific biomolecules (e.g. amino acid, carboxyl group etc.) through specific binding sites on the beads [1, 2, 3] while the chemical modification of their surfaces through coating allows for specificity and high selectivity when used as tagging agents [4, 5]. The inherent magnetic properties and physical characteristics of these beads enable easy manipulation when functionalized with bio-molecules within a magnetic field [1, 5]. This magnetic manipulation is facilitated by the low relative permeability (μ_r) of the fluid which enables strong interaction between the magnetic field and the magnetic-tagged complex [6]. Furthermore, these beads have physical dimensions comparable to some biological entities e.g. Escherichia coli (2µm), red blood cell (6-8µm), the malaria parasite (1-1.2µm) etc. and they are widely available in different sizes from different manufacturers [3, 6]. These numerous benefits have promoted their usage in

Email addresses: olayinka.oduwole@eng.ox.ac.uk (Olayinka Oduwole),
steve.sheard@eng.ox.ac.uk (Steve Sheard).
Corresponding author. Olayinka Oduwole, Tel: +441865 273929,
Email address: olayinka.oduwole@eng.ox.ac.uk

biomedical applications such as immunoassays [1, 5], drug delivery [1, 4, 5], magnetic separation [2, 3, 6], cell transport [2, 6], hyperthermia [1, 5] etc.

Amongst such biomedical applications includes continuous flow magnetic separation, which involves binding bio-molecules to magnetic beads and their continuous separation from a mixture using a magnetic device within microfluidic channels. This concept has been applied to continuously separate magnetic particles from a mixture of magnetic and non-magnetic particles [7, 8], leukocytes from whole blood [9], microphages and tumour cells [10], E. coli bacteria from red blood cell [11] etc.

Magnetic separation is often limited by the formation of magnetic bead agglomerates. Bead agglomerates refer to a cluster of magnetic beads bound by attractive magnetic forces when suspended in fluid. Existing literature has shown that bead agglomerates lead to the blockage of magnetic columns [12], channel clogging and surface adhesion [13], alter the magnetic field properties [11, 14], reduce surface-volume ratio [13] and make it difficult to visualize the attached bio-molecules when viewed under an optical detector [11, 15].

A knowledge of the trajectory pattern of magnetic beads alongside their interaction with neighbouring beads within the magnetic field would aid the manipulation of these beads (or magnetic tagged complexes) within a magnetic separation system which would help to reduce agglomerate formation. Furthermore, the trajectory knowledge is also useful in predicting the behaviour of magnetic beads in diagnostic assays where bead agglomerates are used in detecting bio-molecules such as proteins, virus [16, 17] and for *in vivo* applications (e.g. the micro-magnetic manipulation of magnetic beads to measure the visco-elastic response inside the cytoplasm of a living cell [18, 19], the elastic behaviour of a single DNA molecule [20, 21]).

Herein lies a three dimensional numerical model which predicts the trajectory pattern and interaction among three super-paramagnetic beads suspended in a static fluid placed in a uniform magnetic field. The magnetic interactions among the beads builds upon a similar method introduced earlier in [22, 23] which accounts for the induced magnetization and perturbed field due to the presence of neighbouring beads within a uniform magnetic field. The hydrodynamic interactions was derived using the method of reflection in a vector form (with the lubrication approximation [22, 24, 25]) to account for the change in velocity field within the fluid due to the movement of suspended beads [22, 26, 27].

In this paper, interaction among magnetic beads was observed within a static fluid in the presence of a uniform magnetic field. The uniform magnetic field and static fluid conditions serve as an approximation to the environment within a magnetophoretic system because when magnetic beads are separated within very small separation (on the order of microns), it is possible that they would experience the same magnitude and gradient of magnetic field, then the differences in magnetic drift velocity can be neglected; Also, the velocities of the beads within a static fluid are equivalent to the relative velocities of the beads, if suspended in a moving fluid, due to the laminar flow conditions.

Magnetic bead pair interaction within a magnetophoretic system has been studied by these authors [22, 28] while interaction among chains of magnetic beads have been previously presented in [29, 30]. This study predicts the trajectories of three super-paramagnetic beads within a magnetic separation system which allows for a better understanding of the

agglomeration process. The developed model can predict the build-up of agglomerates from single particles in diagnostic assays requiring a medium bead density (1-10 × 10^6 beads/ml).

2. **Theoretical Model**

When three super-paramagnetic beads are suspended in fluid and placed within a uniform magnetic field, interaction exist among the beads mediated by both the fluid and the magnetic environment, called hydrodynamic interaction and magnetic interaction respectively. The force-equation for the beads is expressed as

$$\sum \mathbf{F} = 0 \tag{1}$$

where **F** is the Force in N. Here, the bold letter indicates a vector. All forces will be considered within a three-dimensional region.

2.1 *Magnetic Force*

There is a translational force which causes a magnetic bead to move in the direction of the magnetic field gradient [22, 23]. Due to the assumption of fast relaxation time of the bead's induced dipole, any rotation of the bead is neglected in this model.

The magnetic force interaction on a bead (e.g. bead 1) due to another bead (e.g. bead *p*, where *p* = 2 or 3) within an external magnetic field is expressed as

$$\mathbf{F_{m1p}} = \int \mu_o((\mathbf{M_1} + \Delta\mathbf{M}_p).\boldsymbol{\nabla})(\mathbf{H_{ext}}(\mathbf{r_1}) + \Delta\mathbf{H}_p)\ \ dV \tag{2}$$

where μ_o is vacuum permeability, $\mathbf{M_1}$ is the magnetization of bead 1 in the absence of other beads in A/m, $\Delta\mathbf{M_p}$ is the induced magnetization due to the presence of bead *p* in A/m, $\mathbf{H_{ext}}$ is the external field in A/m, $\Delta\mathbf{H_p}$ is the perturbed external field due to the presence of bead *p* in A/m, *V* is the volume of bead 1 in m^3 and $\mathbf{r_1}$ is the position vector of bead 1 with respect to the origin [22, 23].

The principle of super-position is used to evaluate the total interaction force on a single bead due to the presence of other beads within the magnetic field (see appendix A).

2.2 *Hydrodynamic Interaction*

Assume bead 1 moves within fluid, the movement generates a velocity field which is transmitted through the fluid. The transmitted velocity field is assumed to be reflected by the *p*th bead (where *p* = 2 or 3) taking into consideration their local velocity fields. The reflected velocity field in turn affects the movement of bead 1 [22, 26, 27].

Hence, solving the Navier-Stokes equation using the method of reflection [22, 26, 27] in a vector form (see Appendix B) and including the lubrication approximation [22, 24, 25, 31],

the hydrodynamic interaction on a bead (e.g. bead 1) due to the presence of other beads within the fluid can be expressed in three dimensions as

$$\mathbf{u_{1p}} = \frac{\frac{(\mathbf{F_h}.\widehat{\mathbf{r_{1p}}})\widehat{\mathbf{r_{1p}}}}{\eta k_a}(1 - k_3k_4) + \left[k_4 + \left(\frac{a_q}{2d_p}\right)(1 - k_3k_4)\right](\mathbf{u_p}.\widehat{\mathbf{r_{1p}}})\widehat{\mathbf{r_{1p}}}}{\left[1 + \left(\frac{a_q}{2d_p}\right)(1 - k_3k_4)\right]}$$

$$+ \frac{(\mathbf{F_h}.\widehat{\mathbf{n_1}})\widehat{\mathbf{n_1}}}{\eta k_a}(1 - k_1k_2) + k_2(\mathbf{u_p}.\widehat{\mathbf{n_1}})\widehat{\mathbf{n_1}}$$

$$+ \frac{(\mathbf{F_h}.\widehat{\mathbf{n_2}})\widehat{\mathbf{n_2}}}{\eta k_a}(1 - k_1k_2) + k_2(\mathbf{u_p}.\widehat{\mathbf{n_2}})\widehat{\mathbf{n_2}} \quad (3)$$

where

$$k_a = 6\pi a_1, k_b = 6\pi a_p \quad (4)$$

$$k_1 = \frac{k_a}{8\pi r_{1p}}, k_2 = \frac{k_b}{8\pi r_{1p}}, k_3 = \frac{k_a}{4\pi r_{1p}}, k_4 = \frac{k_b}{4\pi r_{1p}} \quad (5)$$

$$a_q = \frac{a_h a_g}{a_1} \quad (6)$$

$$a_g = \sqrt{a_1 a_p} \quad (7)$$

$$a_h = \frac{2a_1 a_p}{a_1 + a_p} \quad (8)$$

$$d_p = |d| - (a_1 + a_p) \quad (9)$$

$\mathbf{r_{1p}}$ is the position vector of bead 1 to bead p, $\mathbf{n_1}$ and $\mathbf{n_2}$ are normals to position vector $\mathbf{r_{1p}}$, η is the viscosity in kg/ms, d is the centre-to-centre distance in m, d_p is the gap-distance in m, $\mathbf{F_h}$ is the hydrodynamic force in N, $\mathbf{u_1}$ and $\mathbf{u_p}$ are the velocities of the beads in m/s, a_1 and a_p are the radii of beads 1 and p respectively, a_h is the harmonic mean of both radii and a_g is the geometric mean of both radii.

The hydrodynamic interactions reveal that beads approach each other at lower velocity compared to that predicted by their simple Stokes drag velocity arising from the attractive magnetic force.

2.3 *Sedimentation Force*

The resultant sedimentation force on a single bead is given as

$$\mathbf{F_s} = (\rho_v - \rho_b)V\mathbf{g}\hat{\mathbf{k}} \quad (10)$$

while the sedimentation velocity on a single bead is obtained as

$$\mathbf{u_s} = \frac{(\rho_v - \rho_b)V\mathrm{g}\hat{\mathbf{k}}}{6\pi\eta a} \tag{11}$$

where ρ_v is the density of the fluid in kg/m^3, ρ_b is the density of the bead in kg/m^3, g is the acceleration due to gravity in m/s^2, where the unit vector **k** acts downward in the vertical direction. In this application, the sedimentation force is small (the ratio of the magnetic interaction force to the sedimentation force is of the order of ten to thousand, depending on the separation and magnetization of beads) when compared to the magnetic and hydrodynamic interaction force.

2.4 *Equation of Motion*

Due to low Reynolds number, the magnetic force interaction on bead 1 is balanced by the hydrodynamic force; the velocity of the bead is obtained by inserting the magnetic force into equation 3.

The velocity of bead 1 is then obtained through a vector addition as depicted below.

$$\mathbf{u_1} = \mathbf{u_s} + \sum_{p=2}^{3} \mathbf{u_{1p}} \tag{12}$$

Using the Finite-Time-Finite-Difference (FTFD) scheme, the position of bead 1 is estimated at each time step.

$$\mathbf{r_1}(\mathrm{n}+1) = \mathbf{r_1}(\mathrm{n}) + \mathbf{u_1}(\mathrm{n})\, dt \tag{13}$$

where *dt* is the time step in seconds.

This is repeated for the other two beads in each time step. The numerical model is implemented in Matlab for three super-paramagnetic beads ($2a$ = 1μm, χ = 1.4 [8, 35], ρ_b = 1.7g/cm^3) suspended in water (ρ_v = 1g/cm^3, η = 10^{-3} kgm/s) placed within a uniform magnetic field (**B** = 11mT along the x direction) at room temperature using a time step of 10^{-8}s.

3. **Materials and Methods**

3.1 *Super-paramagnetic Bead*

Super-paramagnetic beads, (Dynal Beads Myone Streptavidin T1), 1μm sized, were purchased from Life Technologies at a concentration of 7-10×10^9 beads/ml. The sedimentation time for this bead in water within a 100μm deep channel is 4.4 minutes.

3.2 *Hydrostatic Fluid Channel*

Counting slides (Fast Read 102 from Immune systems), 85mm by 40mm, with depth 0.1mm were cut into separate hydrostatic fluid channel units for the experiment. Solutions are drawn into the fluid channel by capillary action using an appropriate pipette.

3.3 *Uniform Magnetic Field*

Two rectangular magnets (20mm by 10mm by 5mm N42 Neodymium Magnets) with magnetic field strength of 0.58T were separated by a distance of 55mm and placed in a

position of attraction to create an approximately uniform magnetic field in the middle of their line of centre. The magnetic distribution was modelled in Ansys Maxwell and then measured using a Hall Effect Gauss/Tesla meter (5100 Series Sypris Test & Measurement F.W.Bell 12/04); both measurements predicted a value of 11±0.5mT.

3.4 *Sample Preparation and Bead Tracking*

A solution of super-paramagnetic beads was freshly diluted to a concentration of $7\text{-}10\times10^6$ beads/ml using deionized water. The particles were fully re-suspended and aggregates were broken by placing the solution in an ultrasonic bath for 5 minutes. A volume of 6µl was transferred using an appropriate pipette to the hydrostatic fluid channel. This was placed within the uniform magnetic field distribution by avoiding the edges of the magnets.

The motion and interaction among the beads was recorded using an inverted microscope (Leitz Wetzlar, Germany) with an extended working distance 20× objective lens (Comar Optics, Cambridge, UK) which provided sufficient magnification of the images. These images were recorded using µEye software and a USB digital camera (UEye UI – 2230SE, IDS, Germany) at 33 frames per seconds (fps).

The camera was moved to observe a window (1024 by 768 pixels, where 1 pixel = 0.073µm) where interaction among three isolated super-paramagnetic beads were observed and subsequently recorded. The trajectories of the beads (x-y) were tracked frame by frame using ImageJ software [32].

3.5 *Axial Displacement*

Off-focused images contain information that can be extracted to predict the axial displacement of the super-paramagnetic bead [33, 34]. Prior to the experiment, diffracted images of the bead were obtained at focus and for various defocus distances; the relative height of each bead in the video was then determined by best correlation to the full width half maximum (FWHM) of the intensity distribution (see Figure 6 and Appendix C) with an accuracy of 2µm.

The relative height (z) is combined with the x-y displacement values (from the video data) to predict the beads' trajectories in three dimensions.

4 **Results and Discussion**

4.1 *Three-dimensional Bead Interaction*

For comparison, the three-dimensional simulated trajectory plot was superimposed with the video data (and relative height) as depicted on figures 1 and 2 below. (More results can be found within the Supplementary information section).

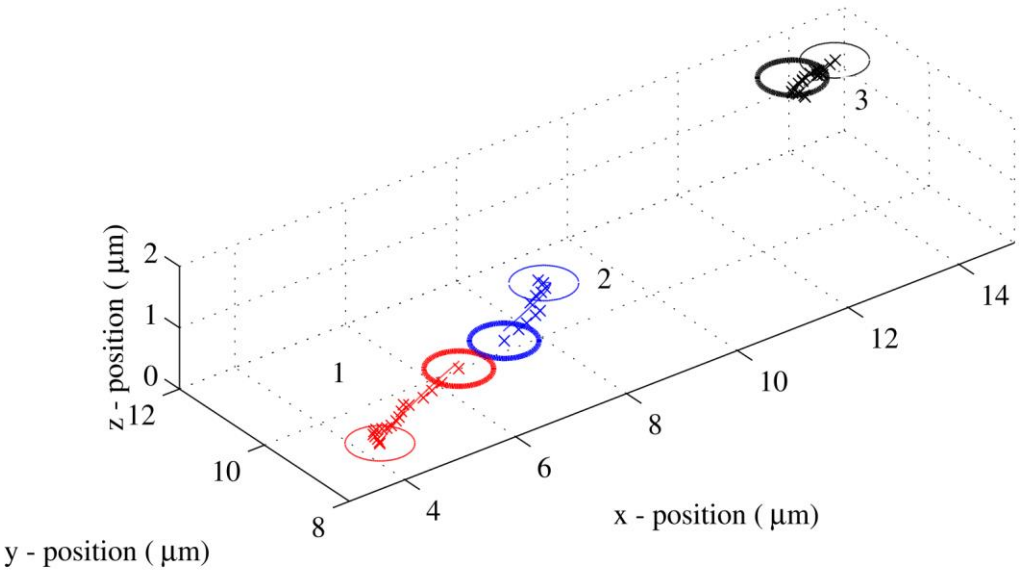

Figure 1. Three-dimensional trajectory of three super-paramagnetic beads, 1µm sized suspended in water (indicated by red, blue and black and labelled as 1, 2 and 3 respectively) under the influence of both magnetic and hydrodynamic interactions within a uniform magnetic field of 11mT in the x direction. The starting points of the beads are indicated by the thin continuous circles while the end points are shown by the thick continuous circles. Experimental data (crosses) are compared with simulation results (continuous line) to validate the model.

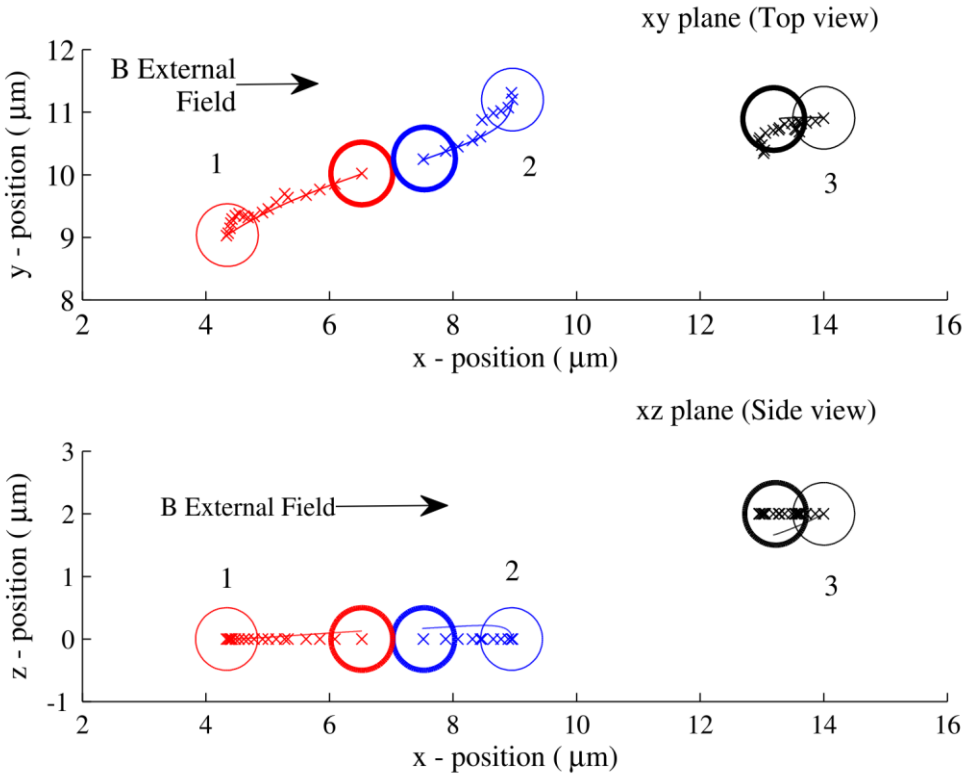

Figure 2. Two dimensional projected trajectory plot (along x-y plane and x-z plane) of three super-paramagnetic beads (indicated by red, blue and black and labelled as 1, 2 and 3 respectively), under the same conditions as figure 1. The starting points of the beads are indicated by the thin continuous circles while the end points are shown by the thick continuous circles. The direction of the magnetic field is indicated by the black arrow on the plot. Experimental data (crosses) are compared with simulation results (continuous line) to validate the model.

Figures 1 and 2 depict the same trajectory plot for three super-paramagnetic beads initially displaced at (4.33, 9.03, 0) µm, (8.96, 11.2, 0) µm and (14, 10.91, 2) µm in three dimensional perspective and two dimensional view respectively. The two-dimensional trajectory plot (see figure 2a) gives the illusion that the second bead is closer to the third bead; this would create a stronger interaction between the second and third beads. However, the height displacement (see figures 1 and 2b) reveals that the second bead is actually closer to the first bead. This leads to a stronger interaction between the first and second beads and the model confirm the observation that the beads come together to form an agglomerate within an approximate time of 0.5s.

If for example, the third bead started at the same height as the first and second beads, then it would be possible to see the second bead strongly interact with the third bead to form an agglomerate.

4.2 *Two-dimensional Interaction of three beads*

The two dimensional trajectory pattern of three beads (under the same conditions described above) was obtained from the simulation and compared with the video data as shown on figure 3 below.

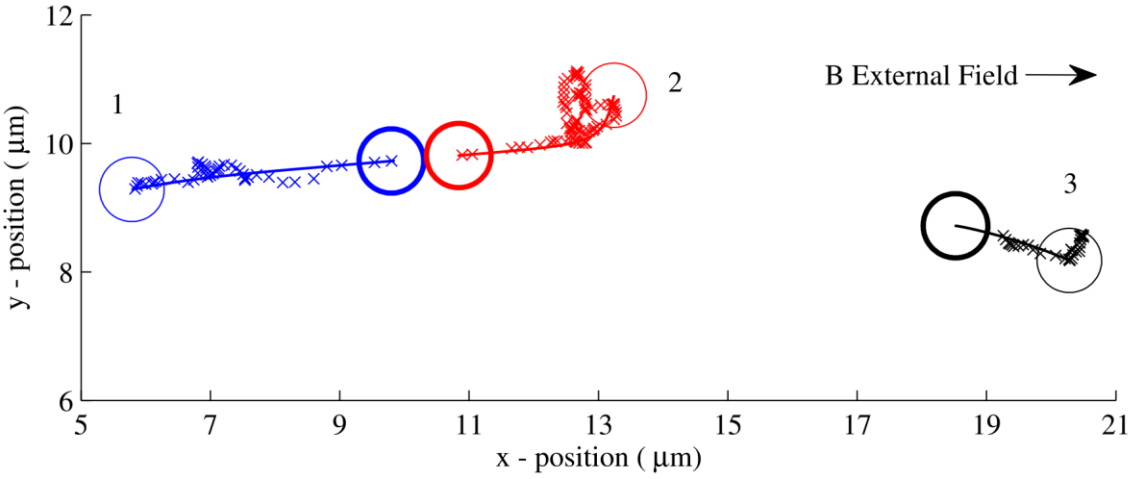

Figure 3. Two-dimensional trajectory plot of three super-paramagnetic beads, 1µm sized suspended in water (indicated by blue, red and black and labelled as 1, 2 and 3 respectively) under the same conditions as figure 1. The starting points of the beads are indicated by the thin continuous circles while the end points are shown by the thick continuous circles. The direction of the magnetic field is indicated by the black arrow on the plot. Experimental data (crosses) are compared with simulation results (continuous line) to validate the model.

Figure 3 shows three beads approximately in a line along the direction of the magnetic field with a separation distance of 7.4µm between the first and the second magnetic beads and 7.5µm between the second and third magnetic beads. At the start of the interaction, the second bead interacts with both the first and third beads, as evident from the curvature of the starting trajectory of the red bead. At this point, the force interaction between the first and second bead approximately balances the force between the second and third beads. The bead displacement during this interval show some random behaviour and is comparable to their expected Brownian rms displacement (0.23 µm) in water (see Appendix D). The dipolar coupling parameter (defined here as the ratio of the magnetic energy to the Brownian energy) is small (0.13-1); this confirms that the beads are displaced by Brownian motion.

As the separation distance between the second and first bead becomes less than 5-6μm, the interaction force becomes stronger and increases steadily from 2 to 2100 times the interaction force between the second and third beads (depending on the separation). At this point, the dipolar coupling parameter increases from 1.7 to 400. Subsequently, the second and first beads approach to form an agglomerate while the second and third beads move apart. The third bead is then displaced by Brownian motion.

The developed model can be applied to study interactions among different sized magnetic beads (or with varying magnetic properties) which could be attached to biological molecules (changing the hydrodynamic diameter). The dipole-dipole interaction force (equation 2) depends on the hydrodynamic radius of the bead (or bead complex) raised to the power of six, square of the effective magnetic susceptibility, square of the applied field strength. As the magnetic field is increased, non-linearities come into play. Furthermore, if the number of beads within the solution is increased, the separation distance among the beads reduces allowing for pair interactions and three-beads interactions and eventually chains of magnetic beads aligned in the direction of the magnetic field.

5. **Conclusion**

A three dimensional vector model was developed in Matlab for predicting magnetic and hydrodynamic interactions among three super-paramagnetic beads placed in a uniform magnetic field.

The relative axial displacement of the super-paramagnetic bead was predicted using the FWHM of the recorded diffracted images of the bead viewed under the optical system.

Results from figures 1 and 2 show that a two dimensional projection does not provide accurate and sufficient information to predict the interactions among beads which could be sedimenting within a micro-channel. This is useful when observing beads within a plane using microscopes.

A good comparison was obtained between the theoretical predictions and video data through the presentation of different bead configurations (see supplementary information section for more results); therefore, the model is a good approximation for predicting a three dimensional trajectory pattern of 1μm magnetic beads interacting within a uniform magnetic field when using a medium bead density (1-10 $\times$ 10^6 beads/ml).

Furthermore, the results showed that the three bead interaction reduces to a bead pair interaction when the magnetic interaction force between a bead pair outweighs the Brownian and sedimentation force on the beads, which occurs when the 1μm beads are separated by a gap distance less than or equal to 6μm, which is consistent with the observations in [22].

The three-dimensional model presented here cannot be used to study interaction between agglomerates once formed. The model only shows the processes involved when particles are coming together to form an agglomerate. The model is being extended to consider particle trajectories beyond the formation of low particle agglomerates.

Acknowledgments

The corresponding author gratefully acknowledges the support of Emmanuel TV for funding.

References

1. M.A.M. Gijs, Magnetic bead handling on-chip: new opportunities for analytical applications, J. Microfluid Nanofluid 1 (2004) 22-40.
2. V. Schaller, U. Kraling, C. Rusu, K. Petersson, J. Wipenmyr, A. Krozer, G. Wahnstrom, A. Sanz-Velasco, P. Enoksson, C. Johansson, Motion of nanometer sized magnetic particles in a magnetic field gradient, J. Appl. Phys. 104 (2008).
3. N. Pamme, Magnetism and Microfluidics, RSC Lab Chip J. 6 (2005) 24-38.
4. M. Mahmoudi, P. Stroeve, A. S, Milani, Nanotechnology Science and Technology, Superparamagnetic Iron oxide Nanoparticles: Synthesis, Surface Engineering, Cytoxicity and Biomedical Applications, nova science publishers, New York, 2011.
5. Q. A. Pankhurst, J. Connoly, S. K. Jones, J. Dobson, Applications of magnetic nanoparticles in biomedicine, J. Appl. Phys. 36 (2003) 167-181.
6. E. P Furlani, Analysis of Particle Transport in a magnetophoretic microsystem, J Appl. Phys. 99 (2006).
7. N. Pamme, A. Manz, On-chip Free Flow Magnetophoresis: Continuous Flow Separation of Magnetic Particles and Agglomerates, Anal. Chem. 76 (2004) 7250-7256.
8. R. Afshar, Y. Moser, T. Lehnert, M.A.M. Gijs, Magnetic particle dosing and size separation in a microfluidic channel, Sensors and Actuators B: Chemical 154 (2011) 73-80.
9. D. W. Inglis, R. Riehn, R. H. Austin, J.C. Sturm, Continuous microfluidic immuomagnetic cell separation, App. Phys. Lett. 85 (2004).
10. N. Pamme, C. Wilhelm, Continuous sorting of magnetic cells via on-chip free-flow magnetophoresis, Lab Chip 6 (2006) 974-980.
11. N. Xia, T. P. Hunt, B. T. Mayers, E. Alsberg, G. M. Whitesides, R. M. Westervelt, D. E. Ingber, Combined microfluidic-micromagnetic separation of living cells in continuous flow, Biomed Microdevices 8 (2006) 299-308.
12. V. Choesmel, P. Anract, H. Hoifodt, J. Thiery, N. Blin, A relevant Immunomagnetic Assay to detect and characterize epithelial cell adhesion molecule-Positive cells in Bone Marrow from patients with Breast carcinoma, American Cancer Society 101 (2004) 693-703.
13. C. Liu, T. Stakenborg, S. Peeters, L. Lagae, Cell manipulation with magnetic particles towards microfluidic cytometry, J. Appl. Phys 105 (2009).
14. N. Wise, T. Grob, K. Morten, I. Thompson, S. Sheard, Magnetophoretic velocities of superparamagnetic particles, agglomerates and complexes, J. Magn. Magn. Mater. 384 (2015) 328-334.
15. R. M. Cooper, D. C. Leslie, K. Domansky, A. Jain, C. Yung, M. Cho, S. Workman, M. Super, D. E. Ingberf, A microdevice for rapid optical detection of magnetically captured rare blood pathogens, Lab Chip 14 (2014) 182-188.
16. Y. Moser, T. Lehnert, M. A. M. Gijs, On-chip immune-agglutination assay with analyte capture by dynamic manipulation of superparamagnetic beads, Lab on a Chip 9 (2009) 3261-3267.
17. Y. Ran, C. Fields, J. Muzard, V. Liauchuk, M. Carr, W. Hall, G. U. Lee, Rapid, highly sensitive detection of herpes simplex virus-1 using multiple antigenic peptide-coated

superparamagnetic beads, Analyst 139 (2014) 6126-6134.
18. A. H. B. de Vries, B. E. Krenn, R. V. Driel, J. S. Kanger, Micro Magnetic Tweezers for Nanomanpulation inside Live Cells, BiophysJ. 88 (2005) 2137-2144.
19. B. G. Hosu, K. Jakab, P. Banki, F. I. Toth, G. Forgacs, Magnetic Tweezers for intracellular applications, Rev. Sci. Instrum. 74 (2003) 4158-4163.
20. C. Gosse, V. Croquette. Magnetic Tweezers: Micromanipulation and Force Measurement at the Molecular Level, BiophysJ. 82 (2002) 3314-3329.
21. S. H. Leuba, T. B. Wheeler, C. Cheng, P. R. LeDuc, M. Fernandez-Sierra, E. Quinones, Structure and dynamics of single DNA molecules manipulated by magnetic tweezers and or flow, MethodsJ. 47 (2009) 214-222.
22. O. Oduwole, D. T. Grob, S. Sheard, Comparison between simulation and experimentally interactions between two magnetic beads in a fluidic system, J. Magn. Magn. Mater. 407 (2016) 8-12.
23. C. Mikkelsen, M. F. Hansen, H. Bruus, Theoretical comparison of magnetic and hydrodynamic interactions between magnetically tagged particles in microfluidic systems, J. Magn. Magn. Mater. 293 (2005) 578-583.
24. S. Yang, L. G. Leal, Y. Kim, Hydrodynamic Interaction between Spheres Coated with Deformable Thin Liquid Films, J. Coll. Int. Sci. 250 (2002) 457-465.
25. L. L. Gary, Advanced Transport Phenomena: fluid mechanics and convective transport processes, first ed., Cambridge University Press, Cambridge, 2007.
26. S. Nasseri, N. Phan-Thien, Hydrodynamic interaction between two nearby swimming micromachines, J. Comp. Mech. 20 (1997) 551-559.
27. J. Happel, H. Brenner, Low Reynolds number in hydrodynamics with special applications in particulate media, first ed., Martinus Nijhoff Publishers, Netherlands, 1983.
28. U. Banerjee, P. Bit, R. Ganguly, S. Hardt, Aggregation dynamics of particles in a microchannel due to an applied magnetic field, J. Microfluid Nanofluid 13 (2012) 565-577.
29. A. Sinha, R. Ganguly, I. K. Puri, Magnetic separation from superparamagnetic particle suspensions, J. Magn. Magn. Mater. 321 (2009) 2251-2256.
30. D. Liu, M. R. Maxey, G. E. Karniadakis, Simulations of dynamic self-assembly of paramagnetic microspheres in confined microgeometries, J. Micromech. Microeng. 15 (2005) 2298-2308.
31. D. Y. C. Chan, R. G. Horn, "The drainage of thin liquid films between solid surfaces", J. Chem. Phys. 83 (1985) 5311-5324.
32. T. Ferreira, W. Rasband, Image J User Guide, FIJI 1.46, October 2012.
33. H. P. Kao, A. S. Verkman, Tracking of Single Fluorescent Particles in Three Dimensions: Use of cylindrical optics to Encode Particle Position, BiophysJ. 67 (1994), 1291-1299.
34. R. Luo, X. Y. Yang, X. F. Peng, Y. F. Sun, Three-dimensional tracking of fluorescent particles applied to micro-fluidic measurements, J. Micromech. Microeng. 16 (2006), 1689-1699.
35. G. Fonnum, C. Johansson, A. Molteberg, S. Morup, E. Alesnes, Characterisation of Dynabeads by magnetization measurements and Mossbauer spectroscopy, J. Magn. Magn. Mater. 293 (2005) 41-47.
36. J. D. Jackson, Classical Electrodynamics, third ed., John Wiley & Sons, New York, Chichester, 1999.

37. J. Suh, M. Dawson, J. Hanes, Real-time multiple-particle tracking: applications to drug and gene-delivery, Adv. Drug Del. Rev. (2005) 63-78.
38. A. Radenovic, Brownian Motion and Single particle Tracking, Advanced bioengineering Laboratory, Ecole Polytechnique Federale De Lausanne, accessed on 30/08/14.

APPENDIX A

Assume a spherical super-paramagnetic bead (e.g. bead 1) lies within an external magnetic field with uniform magnetization over the diameter; the magnetization can be expressed as

$$\mathbf{M_1} = \chi_{eff}\mathbf{H_{ext}};\ \chi_{eff} = \frac{3\chi}{\chi + 3} \quad (A1)$$

where χ is the magnetic susceptibility of the bead [22, 23, 36]. While the perturbed field due to the presence of another bead (say p) is given by [22, 23, 36]

$$\Delta\mathbf{H_p} = \chi_{eff}\frac{a^3}{{r_{1p}}^3} \times \left(\frac{3\left(\mathbf{H_{ext}}.\boldsymbol{r_{1p}}\right)\boldsymbol{r_{1p}}}{{r_{1p}}^2} - \mathbf{H_{ext}}\right) \quad (A2)$$

$$\Delta\mathbf{M_p} = \chi_{eff}\Delta\mathbf{H_p} \quad (A3)$$

It is assumed that there is a linear relationship between the magnetization of the bead and the applied flux density.

When the magnetic interaction on a bead (e.g. bead 1) due to another bead (e.g. bead p, where p = 2 or 3) within an external magnetic field is obtained as $\mathbf{F_{m1p}}$, it is converted into velocity ($\mathbf{u_{1p}}$) using equation 3 (low Reynolds flow).

The principle of superposition is then used to obtain the resultant velocity at bead 1 using equation 12.

APPENDIX B

Neglecting inertia and body force components, Stokes' equation can be expressed as

$$0 = -\nabla p_r + \eta\nabla^2\mathbf{u} \quad (B1)$$

where p_r is the pressure. The method of reflection is used to determine the velocity fields and force between a pair of beads due to the hydrodynamic interactions set up between them. It is only applicable when the beads are separated by a gap distance greater than their physical dimensions.

It assumes that when a bead moves within fluid, the velocity field generated by this movement is transmitted through the fluid; this transmitted velocity field is assumed to be

reflected by the other bead(s) (and considers their local velocity). The reflected velocity field in turn affects the movement of the bead.

The resultant velocity at each bead is then obtained by summing the incident (undisturbed) field with the reflected (disturbed) velocity fields.

The method of reflection relies on two assumptions.

1. A point force acting at the centre of the bead would produce approximately the same velocity field as that of the bead.
2. The drag force obtained from the reflected field at a given bead can be approximated to be equivalent to a uniform velocity whose magnitude and direction is the same as what would exist at the centre of the bead, if it were absent [26, 27].

The method of reflection is linear and subdivides the velocity and pressure into a sum of terms that satisfies the Stokes equation and the boundary conditions. Here, super-scripts represent reflected fields while subscripts represent the beads.

$$\mathbf{v} = \mathbf{v^1} + \mathbf{v^2} + \mathbf{v^3} + \mathbf{v^4} + \cdots (B2)$$

$$p_r = {p_r}^1 + {p_r}^2 + {p_r}^3 + {p_r}^4 + \cdots (B3)$$

where **v** is the fluid velocity [26, 27].

Now, let's consider two beads (with radii a_1 and a_2) moving with velocities $\mathbf{u_1}$ and $\mathbf{u_2}$ in an unbounded fluid, which is stationary at infinity as depicted below.

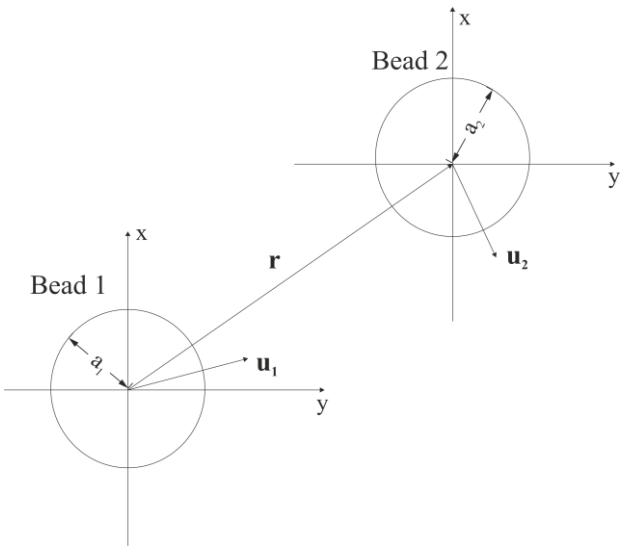

Figure 4. Two beads separated by the position vector **r**, within an x-y coordinate system moving within a viscous fluid with velocities $\mathbf{u_1}$ and $\mathbf{u_2}$ respectively. When bead 1 moves within the fluid, the fluid stream is reflected towards bead 2 and thus affects its movement. The hydrodynamic interaction between the two beads is resolved using the method of reflection.

At Bead 1, the no slip boundary condition [26, 27] gives

$$\mathbf{v^1} = \mathbf{u_1} \quad \text{(B4)}$$

At Bead 2, we assume the fluid stream due to the movement of bead 1 is reflected towards bead 2, this gives

$$\mathbf{v^2} = \mathbf{u_2} - \mathbf{v^1} \quad \text{(B5)}$$

At any arbitrary bead q, the reflected velocity field can be expressed as

$$\mathbf{v_q^2} = \mathbf{u_q} - \mathbf{v^1} \quad (B6)$$

Successive reflections are taken at both beads and we have

$$\mathbf{v^3} = -\mathbf{v^2} \quad \text{(B7)}$$

$$\mathbf{v^4} = -\mathbf{v^3} \quad \text{(B8)}$$

The resultant velocity and drag force for each of the beads is then obtained by summing all the reflected velocities as well as drag forces that satisfied the boundary conditions at the bead's surface [26, 27].

$$\mathbf{F_{h1}} = \mathbf{F_{h1}^{1}} + \mathbf{F_{h1}^{3}} + \mathbf{F_{h1}^{5}} + \cdots \text{(B9)}$$

where $\mathbf{F_h}$ is the long-range hydrodynamic force.

Now, we solve equation B1 and use the boundary conditions outlined in equations B4-B8 to obtain the velocity and drag force between the two beads.

At Bead 1, using Stokes' equation, we have

$$\mathbf{F_{h1}^{1}} = -\eta k_a \mathbf{u_1}, \quad \text{(B10)}$$

where

$$k_a = 6\pi a_1, k_b = 6\pi a_2 \quad (B11)$$

Assume a point force (Equation B10) acts at the centre of the bead, the translational velocity at distances away from the bead is given by

$$\mathbf{v(r)} = k_1 (\mathbf{u_1} + \mathbf{u_1^r}) \quad (B12)$$

$$\mathbf{u_1^r} = \frac{(\mathbf{u_1}.\mathbf{r})\mathbf{r}}{\mathbf{r}^2} \quad (B13)$$

$$k_1 = \frac{k_a}{8\pi r}, k_2 = \frac{k_b}{8\pi r}, k_3 = \frac{k_a}{4\pi r}, k_4 = \frac{k_b}{4\pi r} \quad (B14)$$

The velocity field at bead 2 is then given by

$$\mathbf{u_2^2} = \mathbf{u_2} - k_1 (\mathbf{u_1} + \mathbf{u_1^r}) \quad (B15)$$

Using equation B7, we can then write

$$\mathbf{u_1^3} = k_1 k_2 [(\mathbf{u_1} + 3\mathbf{u_1^r}) \,] - k_2 [(\mathbf{u_2} + \mathbf{u_2^r})] \, (B16)$$

and

$$\mathbf{u_1^5} = (k_1)^2(k_2)^2[(\mathbf{u_1} + 15\mathbf{u_1^r})] - k_1(k_2)^2[(\mathbf{u_2} + 7\mathbf{u_2^r})] \quad (B17)$$

By summing all the odd numbered velocity fields to infinity, we can write the velocity of bead 1 due to hydrodynamic interaction as

$$\frac{\mathbf{F_h}}{\eta k_a} = \frac{\mathbf{u_1} - k_2\mathbf{u_2}}{1 - k_1k_2} + \frac{-k_1k_2\mathbf{u_1^r}}{1 - k_1k_2} + \frac{k_3k_4\mathbf{u_1^r}}{1 - k_3k_4} + \frac{k_2\mathbf{u_2^r}}{1 - k_1k_2} - \frac{k_4\mathbf{u_2^r}}{1 - k_3k_4} \quad (B18)$$

However, when the beads become separated by a gap-distance less than their physical dimensions, the lubrication approximation [22, 24, 25, 31] is used to account for the hydrodynamic interaction. Assume the two beads are separated by a thin gap [25] and approach one another with velocities, $\mathbf{u_1}$ and $\mathbf{u_2}$ respectively in a liquid with viscosity η, bead 1 experiences a lubrication force given by

$$\mathbf{F_{lub}} = -\frac{3\pi\eta a_h a_g}{d_p}[\mathbf{u_1^r} - \mathbf{u_2^r}] \quad (B19)$$

where η is the viscosity in kgm/s, d_p is the gap-distance in m, a_h is the harmonic mean and a_g is the geometric mean in m.

In this model, inter-particle molecular forces are neglected due to the small separation over which they act.

For the special case of considering the hydrodynamic interaction between beads 1 and p in three dimensions (see section 2.2), the velocity of bead 1 is obtained by resolving equations B18 and B19 along the position vector ($\mathbf{r_{1p}}$) and two normal ($\mathbf{n_1}$ and $\mathbf{n_2}$) as given below.

$$\mathbf{u_{1p}} = \frac{\frac{(\mathbf{F_h}.\widehat{\mathbf{r_{1p}}})\widehat{\mathbf{r_{1p}}}}{\eta k_a}(1 - k_3k_4) + \left[k_4 + \left(\frac{a_q}{2d_p}\right)(1 - k_3k_4)\right](\mathbf{u_p}.\widehat{\mathbf{r_{1p}}})\widehat{\mathbf{r_{1p}}}}{\left[1 + \left(\frac{a_q}{2d_p}\right)(1 - k_3k_4)\right]}$$
$$+ \frac{(\mathbf{F_h}.\widehat{\mathbf{n_1}})\widehat{\mathbf{n_1}}}{\eta k_a}(1 - k_1k_2) + k_2(\mathbf{u_p}.\widehat{\mathbf{n_1}})\widehat{\mathbf{n_1}}$$
$$+ \frac{(\mathbf{F_h}.\widehat{\mathbf{n_2}})\widehat{\mathbf{n_2}}}{\eta k_a}(1 - k_1k_2) + k_2(\mathbf{u_p}.\widehat{\mathbf{n_2}})\widehat{\mathbf{n_2}} \quad (B20)$$

where

$$a_q = \frac{a_h a_g}{a_1} \quad (B21)$$

$$d_p = |d| - \left(a_1 + a_p\right) \quad (B22)$$

APPENDIX C

A solution of super-paramagnetic bead (Dynal Beads Myone Streptavidin T1) was prepared at a concentration of 7-10×10^2 beads/ml. 6µl of this solution was placed on a microscope glass slide (iMED) using an appropriate pipette.

This was then viewed under the setup described in section 3.4 (in the absence of the magnets). The stage vernier scale was used to determine the defocus position in µm. The microscope sample stage was moved vertically until a single bead appeared in focus, translated up and down for the various defocus distances. The focussed and defocused images were then recorded and post-processed using imageJ [32].

The images are displayed below (above focus only).

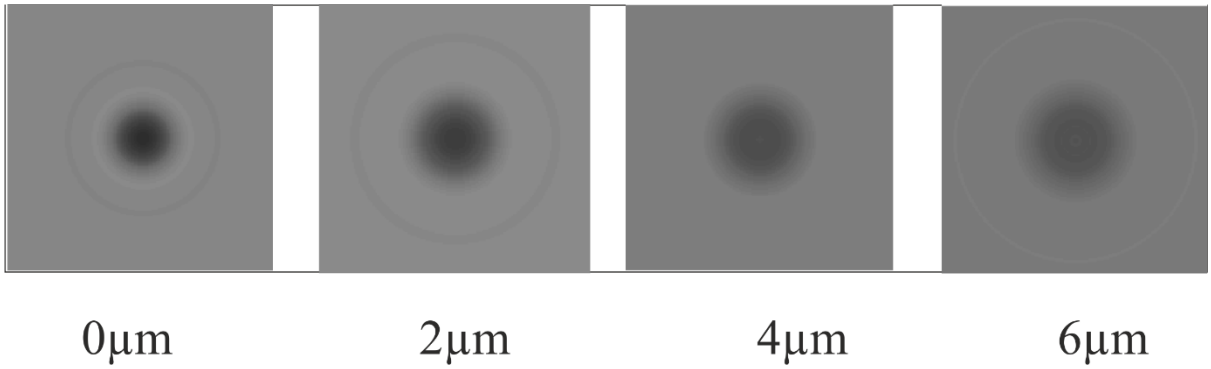

Figure 5. Post-processed images of 1µm super-paramagnetic beads (myone Dynal Beads Streptavidin T1 obtained from Life Technologies) viewed under the optical microscope at different axial positions.

In order to improve the quality of recorded images, the images were exported into Matlab and the following smoothing procedure was undertaken, following the steps of Luo et al [34]. The centroid was determined by manual observation. A line was projected out from the centroid across the image; the line was divided into a number of points. Smoothing was obtained by rotating the radial line by 360 degrees and taking an average of the intensity values at each radial distance points.

The intensity distribution of the bead at various distances (above focus) was normalized by the intensity value at focus and depicted below in figure 6.

For every image, the relative height (z) of each bead in the video was determined by best correlation to the full width half maximum (FWHM) of the intensity distribution in figure 6.

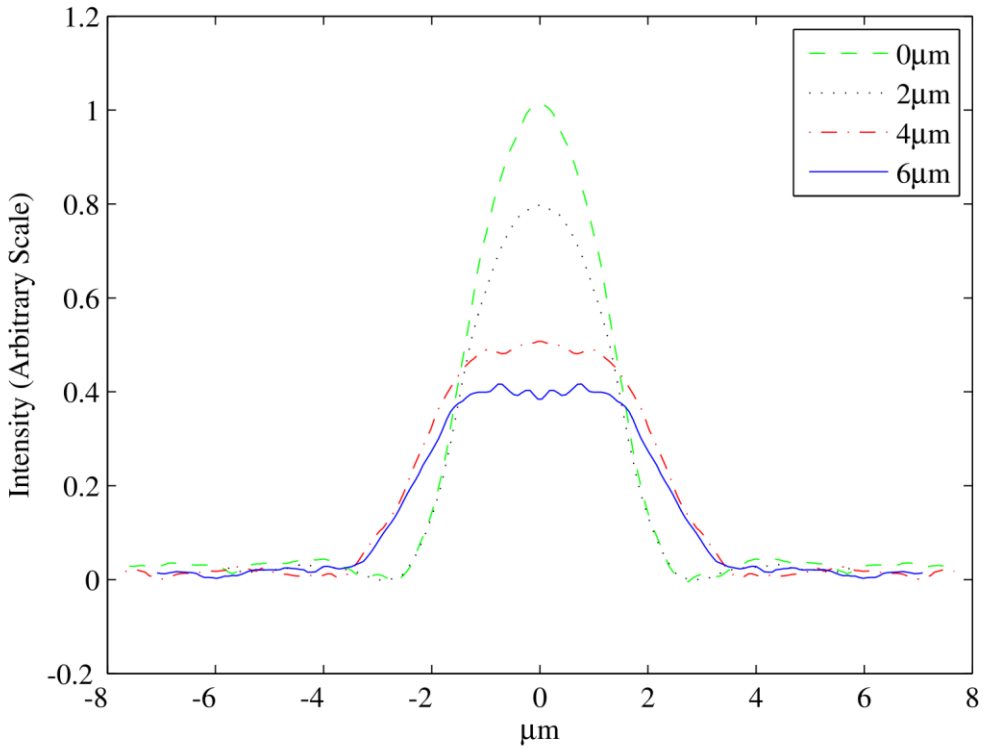

Figure 6. Normalized intensity distribution of a 1µm super-paramagnetic bead (Myone Dynal Beads Streptavidin T1) viewed under the optical microscope at focus (in green dash line) and various distances with respect to the focal plane (2µm in black dotted line, 4µm in red dash-dot line and 6µm in blue continuous line).

APPENDIX D

Using Stokes' Einstein relation [37, 38], the diffusion coefficient is given as

$$D_f = \frac{kT}{6\pi\eta a} \qquad (D1)$$

While the Brownian displacement of a bead is expressed below [37, 38]

$$< \Delta r^2(t_s) >_{2D} = 4\, D_f\, dt \qquad (D2)$$

where k is the Boltzmann constant, T is the temperature and dt is the time step in s. For a bead (1µm diameter) suspended in water (η=10^{-3}kg/ms) at room temperature, the rms displacement is estimated as 0.23µm using a time step of 0.03s.

The dipolar coupling parameter is defined as the ratio of the magnetic energy to the Brownian energy.